Lithium Intercalation into Vanadium Pentoxide: a Theoretical Study

J. S. Braithwaite,*,† C. R. A. Catlow,† J. D. Gale,‡ and J. H. Harding§

The Royal Institution of Great Britain, 21 Albemarle Street, London W1X 4BS, U.K., Department of Chemistry, Imperial College, Exhibition Road, London SW7 2AZ, U.K., and Department of Physics, University College London, Gower Street, London WC1 E6BT, U.K.

Received July 20, 1998. Revised Manuscript Received May 20, 1999

The atomic and electronic structures of three $Li_xV_2O_5$ phases have been investigated using plane wave calculations based on density functional theory. We show that reduction of the vanadium ions occurs during lithium intercalation. At low lithium concentrations this reduction is limited to specific ions. Changes to unit cell dimensions can be predicted correctly. Calculated cell potentials are in good agreement with experiment. Initial "atomistic" calculations were successfully used to find the most stable sites for lithium in the V_2O_5 lattice. Calculated activation energies suggest that lithium is highly mobile along the 010 direction.

1. Introduction

In the last 20 years, there has been an increasing interest in a new type of rechargeable battery that relies on the reversible intercalation of small metal cations, such as Li^+, into transition metal oxides without chemical bond cleavage. These batteries exhibit high charge densities, and the reversible nature of the process leads to good cycling properties: both attributes make these cells very economically attractive. Solid-state lithium batteries are already being used in some laptop computers and mobile phones, where size and weight are at a premium. For the same reasons, electric vehicles are a future application with much promise.

The cells typically use a lithium anode (either as the pure metal, a compound, or, most commonly, a graphite bronze) and a transition metal oxide as the cathode. Organic[1] polymers, with good ionic conducting properties, are now being used as the electrolyte. Examples of promising cathode hosts include CoO_2,[2] $LiMn_2O_4$,[3,4] and the subject of this study: V_2O_5. These materials all have structures with either 2-D layers or 3-D cavities that allow the intercalation of small metal cations. The potential difference between the anode and cathode with respect to lithium leads to initial cell voltages in the region of 3−4 V,[5] as the intercalation reaction, where Li^+ ions move from the anode, through the electrolyte, and into the cathode host, is energetically strongly favorable at room temperature. Battery charging, therefore, corresponds to the deintercalation reaction.

The overall intercalation reaction in V_2O_5 is as follows:

$$V_2O_5 + x\mathrm{Li} = \mathrm{Li}_xV_2O_5$$

During the intercalation reaction, electrons are also introduced into the cathode of the battery system to balance the positive charge of the lithium ions, and it is therefore important that the cathode is either an electronic conductor or has a conducting material, such as graphite, added to it. A number of ab initio studies,[6−9] using DFT on a range of transition metal oxide cathode materials, suggest that the intercalated lithium is fully ionized and that this charge is transferred to the transition metal centers and, to a degree, to the oxygen atoms. The location, in the Li/V_2O_5 system, of the electrons due to the intercalated lithium will be investigated in our work.

V_2O_5 was first suggested as a cathode material in the 1970s[10] and has since undergone extensive experimental study.[11−16] Several $Li_xV_2O_5$ phases have been reported over a range of temperatures and lithium concentrations; the effect of lithium intercalation on the structure of the oxide is, therefore, also examined in this study.

The central aims of this work are, first, to increase the understanding, at the atomic level, of the structural

† The Royal Institution of Great Britain.
‡ Imperial College.
§ University College London.

(1) Meyer, W. H. *Adv. Mater.* **1998**, *10*, 439−449.
(2) Amatucci, G. C.; Tarascon, J. M.; Klein, L. C. *J. Electrochem. Soc.* **1996**, *143*, 1114.
(3) Bruce, P. G.; Armstrong, A. R.; Huang, H. T. *J. Power Sources* **1997**, *68*, 19−23.
(4) Xia, Y.; Yoshio, M. *J. Electrochem. Soc.* **1996**, *143*, 825−833.
(5) West, K.; Zachau-Christiansen, B.; Jacobsen, T.; Skaarup S. *Solid State Ionics* **1995**, *76*, 15−21.
(6) Ceder, G.; Chiang, Y.-M.; Sadoway, D. R.; Aydinol, M. K.; Jang, Y.-I.; Huang, B. *Nature* **1998**, *392*, 694−696.
(7) Aydinol, M. K.; Ceder, G. *J. Electrochem. Soc.* **1997**, *144*, 3832−3835.
(8) Benco, L.; Barras, J.-L.; Daul, C. A.; Deiss, E. *Inorg. Chem.* **1999**, *38*, 20−28.
(9) Aydinol, M. K.; Kohan, A. F.; Ceder, G.; Cho, K.; Joannopoulos, J. *Phys. Rev. B* **1997**, *56*, 1354−1365.
(10) Day, A. N.; Sullivan, B. P. U.S. Pat. 3,655,585, 1972.
(11) Cava, R. J.; Santoro, A.; Murphy, D. W.; Zahurak, S. M.; Fleming, R. M.; Marsh, P.; Roth, R. S. *J. Solid State Chem.* **1986**, *65*, 63−71.
(12) West, K.; Zachau-Christiansen, B.; Jacobsen, T.; Skaarup S. *Electrochim. Acta.* **1993**, *38*, 1215−1220.
(13) Cocciantelli, J. M.; Menetrier, M.; Demas, C.; Doumerc, J. P.; Pouchard, M.; Broussely, M.; Labat, J. *Solid State Ionics* **1995**, *76*, 143−150.
(14) Prouzet, E.; Cartier, C.; Villain, F.; Tranchant, A. *J. Chem. Soc., Faraday Trans.* **1996**, *92*, 103−109.
(15) Vivier, V.; Farcy, J.; Pereira-Ramos, J.-P. *Electrochemica Acta* **1998**, *44*, 831−839.
(16) Zhang, J.-G.; Liu, P.; Turner, J. A.; Tracy, C. E.; Benson, D. K. *J. Electrochem. Soc.* **1998**, *145*, 1889−1892.

10.1021/cm980735r CCC: $18.00
Published on Web 07/14/1999

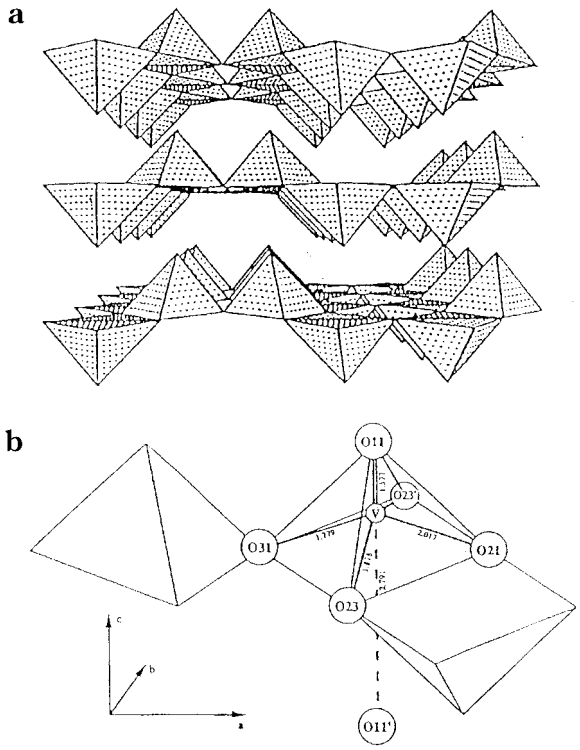

Figure 1. V_2O_5 structure: (a) layers; (b) coordination around the vanadium.[18]

and electronic changes that take place during intercalation and, second, to model the thermodynamics of the intercalation reaction. A detailed prediction of cell voltages, with comparison to electrochemical data will be made in future work; initial results are, however, presented here. The atomistic and electronic structure methods used are discussed and comparisons made in terms of accuracy and computational cost. The structural chemistry and theoretical methods are outlined first before presentation and discussion of results.

2. Experimental Background

2.1. Structural Properties. *2.1.1. Vanadium Pentoxide.* The layer structure of V_2O_5, shown in Figure 1, is a major factor in making the material such an effective host for this type of insertion reaction. It is therefore important that the computational methods used reproduce this structure accurately and that any structural changes on lithium intercalation can also be modeled correctly. The oxide has a structure made up of octahedra joined by edge and corner sharing. These octahedra are distorted to such a large extent that it has been suggested that V_2O_5 is better represented with square-based pyramidal units.[17]

The electrostatic repulsion between neighboring vanadium atoms results in the vanadium atoms being displaced away from the base of each pyramid and toward the apical oxygen. This displacement produces a short vanadyl bond, at only 1.577 Å, from the vanadium atom to this oxygen. The longest V−O bond is trans to the vanadyl V═O and, at 2.791 Å, is essentially ionic.

2.1.2. Lithiated Phases. $Li_xV_2O_5$ system can adopt many phases depending on temperature and lithium concentration, x; the phase diagram for the system is shown in Figure 2.

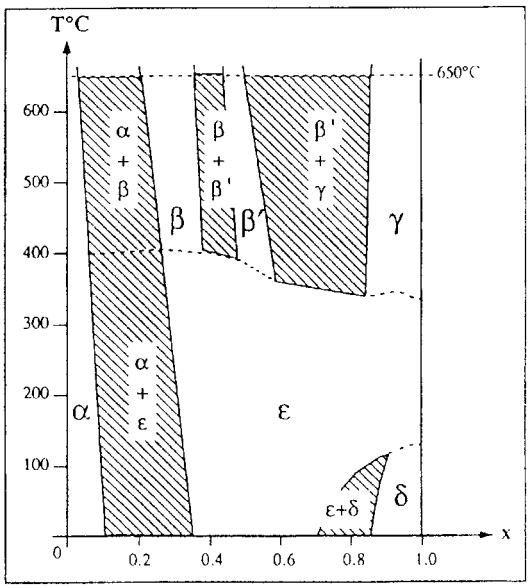

Figure 2. Phase diagram for $Li_xV_2O_5$.[19]

Some phases, such as α-$Li_xV_2O_5$ and ϵ-$Li_xV_2O_5$, involve very little structural distortion of the bulk oxide, while others, such as β-$Li_xV_2O_5$, have a square-based pyramidal arrangement, which is significantly different from that in V_2O_5.[19] The α phase, which has a low lithium content ($x \leq 0.1$) and the ϵ phase ($0.35 \leq x \leq 0.70$) are both stable at temperatures below 400 °C. The only distortion of the V_2O_5 structure is a slight puckering of the pyramidal units parallel to the a direction, which results in a reduction of the cell parameter in that direction, an effect that becomes more pronounced as the lithium concentration increases. ϵ-$Li_xV_2O_5$ also shows a steady expansion of the c lattice parameter as x increases, due to the increased concentration of lithium between the V_2O_5 layers. β-$Li_xV_2O_5$, which occurs at higher temperatures than α or ϵ and with $0.22 \leq x \leq 0.49$, is considerably distorted so that the square-pyramidal units form tunnels within the lattice.[5] The layered structure of bulk V_2O_5 is totally disrupted.

Our present theoretical study is confined to energy calculations of static structures at 0 K; therefore, we focus on changes that occur to the dimensions of the unit cell as lithium is introduced into the oxide, which we relate to experiment. The investigation of temperature effects is reserved for further studies.

2.2. Electrochemical Data. Many electrochemical studies have been carried out on test cells containing various phases of $Li_xV_2O_5$. West et al. have found that, at 100 °C, it is possible to intercalate Li^+ electrochemically into the α phase over a lithium composition range which is far wider than the thermodynamically stable range given above.[5] They find that it is possible to incorporate up to just under three lithium atoms per V_2O_5 formula unit. The α phase seems to cycle reversibly for $0.0 \leq x \leq 1.0$, which corresponds to a cell voltage change from 3.5 to 2.75 V relative to a cell anode of solid lithium. The voltage curve, shown in Figure 3, exhibits two distinct plateaux, at 3.4 and 3.2 V, an indication of two distinct Li sites in the host V_2O_5 lattice.

It is possible to discharge the test cell down to 2.2 V, which corresponds to $x = 1.8$, and still reversibly remove

(17) Enjalbert, R.; Galy, J. *Acta Crystallogr.* **1986**, *C42*, 1467−1469.

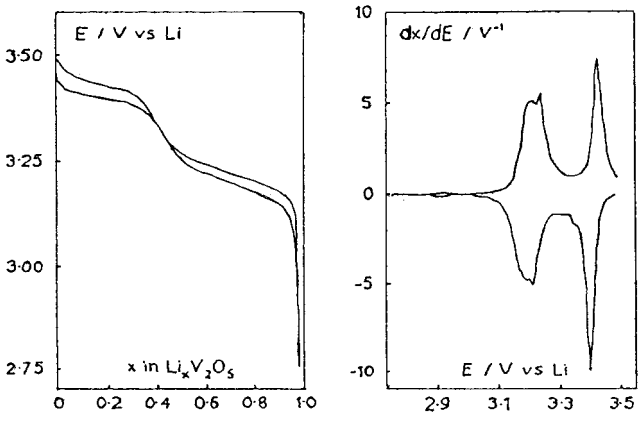

Figure 3. Experimental voltage curve for a Li/V_2O_5 test cell.[5]

the lithium when recharging. Further discharge past this point results in an irreversible structural transformation to the ω-phase where some of the intercalated lithium is strongly bonded to the host oxide and cannot be electrochemically removed.

3. Theoretical Methods

Two approaches have been used in this study: the first employs interatomic potentials with static lattice minimization; the second uses electronic structure techniques based on density functional theory. We show that these two methods often complement each other; atomistic simulation can be used to guide more computationally expensive electronic structure work while the latter can be used to check the accuracy of the first.

3.1. Atomistic Simulation Methods. All the atomistic modeling has been carried out using the GULP code, developed by Gale,[21] which can be used to carry out both static lattice simulations for bulk and defective systems. A wide range of physical properties (e.g. elastic and dielectric constants) and lattice dynamical properties can be calculated for the optimized geometry.

The static lattice model divides interatomic forces into two components: Coulombic and short range. The Coulombic interactions are calculated using the Ewald method,[22] where the conditionally convergent Madelung sum can be solved by carrying out the summation in both real and reciprocal space. Short-range forces are modeled using two different potential functions: the Buckingham and Morse potentials. These potential functions contain parameters that are derived by fitting to experimental data or calculated using ab initio techniques.

The potential model for V_2O_5 was developed by Dietrich et al.[18] by fitting to the experimental crystal structure and physical properties such as elastic constants. They use Buckingham potentials to model most interatomic interactions and a Morse potential to reproduce the short V═O vanadyl bond. This Morse potential and the very repulsive Buckingham potential, which models the weak V···O ionic bond, reproduce the layered structure of the oxide by significantly distorting the V−O octahedra. Consequently, the set of potentials is specific to this material and they cannot be used to model a different vanadium oxide. The short-range forces between O ions were modeled using a Buckingham potential derived previously,[23] while all V−V short-range interactions are ignored, as they are assumed to be insignificant at the interatomic separations in the crystal due to the relative sizes of the V^V and O^{2-} ions. In the lithium bronzes, Li−O interactions are modeled with a Buckingham potential that has been fitted to the structure of lithium oxide:[24] we can accurately reproduce the Li_2O structure with the Li−O and O−O interatomic potentials used in this work. A Buckingham potential, derived from empirical fitting to the structure of V_6O_{13}, is used to include V^{IV}−O interactions. The potential force field parameters that are used in this study are shown in Tables 1−3.

Table 1. Buckingham Potential Parameters and Shell Model Parameters Used in This Study[a]

interaction	A/eV	ρ/Å	C/eVÅ^6	q_{core}/|e|	k/eV Å^2
$V^V-O_{equatorial}$	5312.99	0.26797	0.00	5.00	∞
$V^V\cdots O_{axial}$	2549.73	0.34115	0.00	5.00	∞
$V^{IV}-O$	1290.56	0.34039	0.00	4.00	∞
O−O	22764.30	0.14900	23.00	0.717	54.952
Li−O	828.01	0.27930	0.00	1.00	∞

[a] Buckingham potential has the following form: $\Psi_{ij}(r) = A_{ij}\exp(-r_{ij}/\rho) - C_{ij}/r_{ij}^6$.

Table 2. Buckingham Potential Cutoffs Used in This Study

interaction	r_{min}/Å	r_{max}/Å
$V^V-O_{equatorial}$	0.00	10.00
V^V-O_{axial}	1.99	10.00
$V^{IV}-O$	0.00	10.00
O−O	0.00	10.00
Li−O	0.00	10.00

Table 3. Morse Potential and Cutoffs Used in This Study[a]

interaction	D_0/eV	α/Å^{-1}	r_0/Å	r_{min}/Å	r_{max}/Å
$V{=}O_{axial}$	10.00	2.302170	1.584	0.00	1.99

[a] Morse potential has the following form: $\Psi_{ij}(r) = D_0(\{1 - \exp[\alpha(r - r_0)]\}^2 - 1)$.

The lattice energy of the crystal system is minimized using a *quasi*-Newton−Raphson optimization procedure. Crystalline systems are simulated using periodic boundary conditions, for which cell parameters can be optimized, as well as atomic positions. The shell model[25] has been used to include the effects of ionic polarization within the bulk lattice. To model the sites and energetics of intercalated Li^+ ions, defect calculations have been carried out according to the scheme of Mott and Littleton,[26] which divides the lattice around the defect into different regions: in the inner region around the defect center, atomic positions are optimized explicitly, and the atoms surrounding this region are treated by *quasi*-continuum methods.

3.2. Electronic Structure Methods. We have used density functional theory[27−29] to undertake electronic

(18) Dietrich, A.; Catlow, C. R. A.; Maigret, B. *Mol. Simul.* **1993**, *11*, 251−265.
(19) Galy, J. *J. Solid State Chem.* **1992**, *100*, 229−245.
(20) Murphy, D. W.; Christian, P. A.; DiSalvo, F. J.; Waszczak, J. V. *Inorg. Chem.* **1979**, *18*, 2800.
(21) Gale, J. D. *J. Chem. Soc., Faraday Trans.* **1997**, *93*, 629.
(22) Ewald, R. P. *Ann. Phys.* **1921**, *64*, 253.
(23) Catlow, C. R. A. *Proc. R. Soc. London* **1977**, *A353*, 533−561.
(24) Binks, D. J. Ph.D. Thesis, Chemistry Department, University of Surrey, Oct 1994.
(25) Dick, B. G.; Overhauser, A. W. *Phys. Rev* **1958**, *112*, 90.
(26) Mott, N. F.; Littleton, M. J. *Trans. Faraday Soc.* **1938**, *34*, 485.

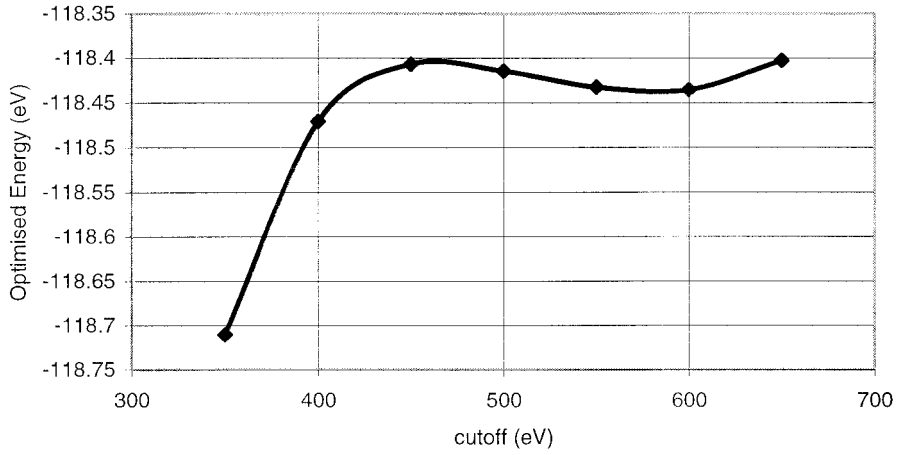

Figure 4. Dependence of optimized energy on plane wave cutoff.

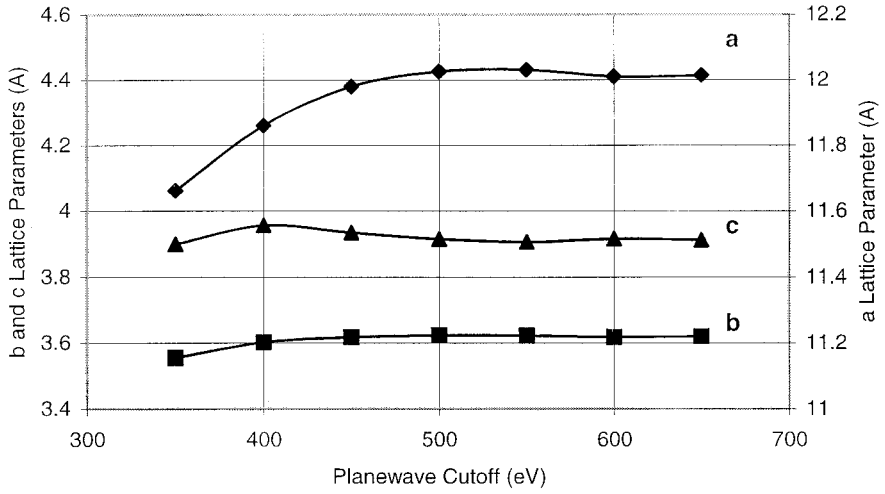

Figure 5. Dependence of optimized lattice parameters of V_2O_5 on plane wave cutoff.

structure calculations employing periodic boundary conditions, utilizing the Vienna Atomistic Simulation Package (VASP).[30,31] DFT plane wave pseudopotential methods have recently been successfully used to model lithium vanadate materials.[9,32,33]

Due to the periodic nature of the crystal system, the single-electron wave functions may be represented by plane waves. In practice, the infinite number of plane waves required is limited to a finite number, with a specified energy cutoff, and pseudopotentials are used to represent the tightly held core electrons in the system. Only the valence electrons are expanded as plane waves, which means that the energy cutoff and the cost of the calculation can be relatively low. The generalized gradient correction (GGA)[34−36] to the local density approximation (LDA)[37] has been shown to give better estimates of binding energies than LDA alone, and the spin-polarized version has been used in all the work presented here. We have made use of ultrasoft pseudopotentials[38] to keep the plane wave cutoff to a minimum. A conjugate gradient minimizer is used to solve self-consistently the Kohn−Sham equations[28] to give the minimum total energy for a given structure.

Initially our work focused on ensuring that our methods correctly reproduced the V_2O_5 structure and on deciding on a suitable plane wave cutoff for the main body of work. As the total energy of the system should converge as the plane wave cutoff energy is increased, the correct cutoff for the system can be found by carrying out a series of geometry optimizations of the V_2O_5 structure with increasing cutoff. By comparison of the resulting total energies and geometries, a cutoff can be selected that balances accuracy with computational cost. The dependence of the total energy and the unit cell dimensions on plane wave cutoff are given in Figures 4 and 5.

While the optimized total energies appear to oscillate above a cutoff of 450 eV there is still convergence within 0.05 eV; also the V_2O_5 structure converges at a cutoff of around 500 eV. On the basis of these results, we have used a plane wave cutoff of 550 eV in this work, as it is energy differences and not absolute values that are of interest to us.

(27) Hohenberg, P.; Kohn, W. *Phys. Rev. A* **1964**, *136*, 864.
(28) Kohn, W.; Sham, L. *Phys. Rev. A* **1965**, *140*, 1133.
(29) Ziegler, T. *Chem. Rev.* **1991**, *91*, 651−667.
(30) Kresse, G.; Furthmuller, J. *Phys. Rev. B* **1996**, *54*[11], 169.
(31) Kresse, G.; Furthmuller, J. *Comput. Mater. Sci.* **1996**, *6*, 15.
(32) Benedek, R.; Thackeray, M. M.; Yang, L. H. *Phys. Rev. B* **1997**, *56*, 10707−10710.
(33) Ceder, G.; Aydinol, M. K.; Kohan, A. F. *Comput. Mater. Sci.* **1997**, *8*, 161.
(34) Perdew, J. P. *Phys. Rev. B* **1986**, *33*, 8822.
(35) Perdew, J. P.; Wang, Y. *Phys. Rev. B* **1992**, *46*, 6671.
(36) White, J. A.; Bird, D. M. *Phys. Rev. B* **1994**, *50*, 4954.
(37) Perdew, J. P.; Zunger, A. *Phys. Rev. B* **1981**, *23*, 5048.
(38) Vanderbilt, D. *Phys. Rev. B* **1990**, *41*, 7892.

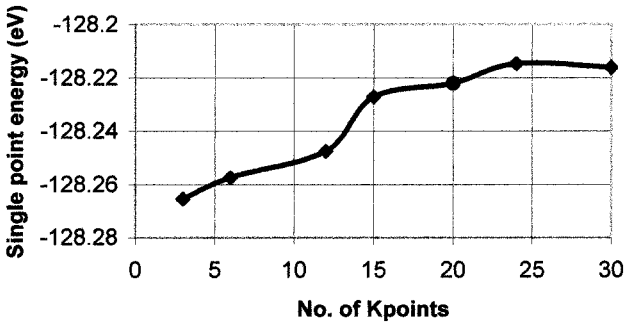

Figure 6. The dependence of the single point energy of $Li_2V_2O_5$ on the number of *k*-points used in the calculation.

Table 4. Calculated Structure of V_2O_5

observable	experiment[17]	calculation	error (%)
a lattice parameter (Å)	11.512	11.698	1.62
b lattice parameter (Å)	3.564	3.587	0.65
c lattice parameter (Å)	4.368	4.471	2.36
V═O, vanadyl (Å)	1.577	1.607	1.90
V···O, ionic (Å)	2.793	2.865	2.58

As the concentration of intercalated lithium increases, the electrical conductivity of the $Li_xV_2O_5$ system improves and therefore the number of *k*-points required to sample accurately the Brillouin zone is greater. The convergence of total energies with an increasing number of *k*-points has been examined with a series of single point calculations on $Li_2V_2O_5$, the most highly lithiated phase in this work. The results (Figure 6) show that the number of *k*-points has a small effect on the value of the total energy with convergence occurring at around 20 *k*-points: we have taken this value for the main body of our work as it keeps the resources needed for the calculations to a manageable size.

As the present work concentrates on energy differences and not on absolute values, the effect of any systematic errors that are present is reduced. Calculated lattice parameters and selected bond lengths of the optimized V_2O_5 structure are compared to experiment in Table 4. There is acceptable agreement between the two.

4. Results and Discussion

Initially, we present results from a series of defect calculations using interatomic potential-based methods, which have been used to find the most stable lithium sites in the V_2O_5 lattice. These results are then used to give starting geometries for electronic structure calculations on a range of $Li_xV_2O_5$ phases, giving information on the structural changes induced by lithium intercalation, thermodynamic properties, and the electronic structure of the lithiated phases. Finally, we return to the atomistic calculations to study lithium migration processes in the V_2O_5 lattice.

4.1. Low Energy Lithium Sites. The atomistic simulation method, within the Mott-Littleton approximation, was first used to identify low energy sites for Li^+ within the V_2O_5 lattice. We note that the calculated energies correspond to the change that occurs when an isolated Li^+ ion is introduced into the infinite V_2O_5 lattice; hence, the effects of Li^+-Li^+ interactions are not included in this calculation. Such calculations do not model the changes in the unit cell dimensions that will occur when lithium is intercalated into V_2O_5 but serve as a good guide to the positions that the Li^+ ions will occupy in the oxide, especially at low lithium concentrations and, as such, provide good starting geometries for the lithium ions in the subsequent electronic structure work. The defect energies of 15 interstitial Li^+ sites have been calculated in this way. Explicit relaxation of the ions closest to the defect, within a region with a radius of 8 Å containing around 300 atoms, gives accurate defect energies. The dependence of these defect energies on this region size has been investigated and found to be convergent at around 7−8 Å. The lowest energy sites identified by the calculations are given in Table 5 and shown graphically in Figure 7.

Table 5. Low Energy Lithium Sites in V_2O_5

ref. no.	lithium position (fractional coordinates)	defect energy (eV)
1	0.5047, 0.0040, 0.3976	−8.19
2	0.5000, 0.2588, 0.3447	−7.60
3	0.5049, 0.5010, 0.4147	−7.38

The similarity in the energy of these positions indicates that the intercalated lithium is likely to adopt more than one position in the bulk lattice and suggests that there is a flat potential energy surface and, therefore, Li^+ mobility along the *b* direction: essentially the Li^+ ions are located along this channel. We will investigate this feature in more detail later.

4.2. $Li_xV_2O_5$ Geometry Optimization. Full geometry optimizations have been carried out using the DFT techniques for a range of lithium concentrations in V_2O_5, yielding information about structural modifications, charge density distribution, and cell voltages.

Each $Li_xV_2O_5$ phase has been simulated by varying the number of lithium ions in a single unit cell of V_2O_5. Geometries have been optimized with *P*1 symmetry and with all unit cell dimensions and angles free to vary. In each case, the initial structure for V_2O_5 is that of the optimized host lattice, while the starting coordinates of the lithium atoms in the V_2O_5 host have been varied to check that the global minimum has been found. The most stable structures for each $Li_xV_2O_5$ phase are given in Figure 8.

The changes to the lattice parameters, as the lithium content is increased, are given in Figure 9. The calculated data reproduce the general trends seen in experiment (shown in Figure 9), for $0 \leq x \leq 1$. The increase in the *c* lattice parameter, as the lithium content increases, is reproduced by the calculations although this effect is somewhat overestimated: the changes in *a* and *b* are accurately modeled by the simulations. A more detailed comparison will be made in a future paper, where the results from a greater number of $Li_xV_2O_5$ simulations will be presented, but it is clear from the present calculations that the DFT technique employed is able to reproduce well the structural changes accompanying intercalation reactions.

The lithium positions that are predicted by the electronic structure calculations, shown in Table 6, can be compared to the results from the atomistic defect calculations in Table 5. Good agreement is found along the *a* and *c* axes, while the difference along *b* will be explained by the flatness of the potential energy profile for lithium in this direction.

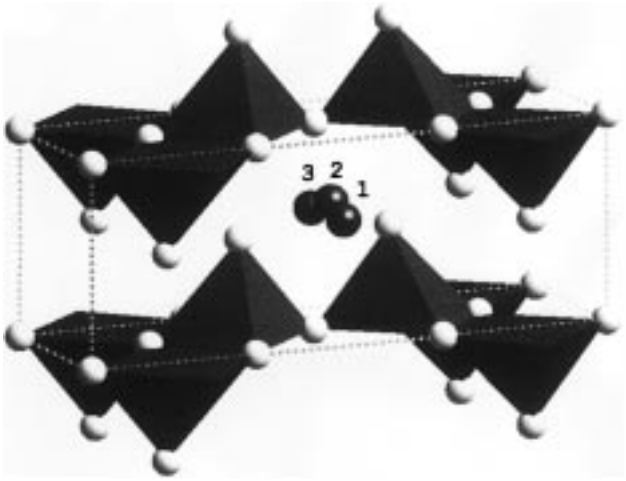

Figure 7. Low-energy lithium sites within V_2O_5. Site reference numbers refer to Table 5.

Atomistic calculations are clearly useful tools for finding initial starting configurations for more costly quantum mechanical studies, especially when dealing with complex systems, for which identification of the global energy minimum of the system is more difficult. Substantial savings in computational cost can be made, as some configurations of the system can be rejected quickly using atomistic techniques.

4.3. Cell Potentials. The calculation of cell potentials and the reproduction of the experimental cell discharge curve are important aims of this work. We present initial results that show the validity of our simulations, as applied to this problem.

In this study, as in previous work by other authors,[9,39] the average cell voltage can be estimated from the following well-known relationship:

$$\Delta G = -nFE_{\mathrm{CELL}}$$

In the following reaction:

$$\mathrm{Li}_y\mathrm{V}_2\mathrm{O}_5 + x\mathrm{Li}_{(s)} \rightarrow \mathrm{Li}_{x+y}\mathrm{V}_2\mathrm{O}_5$$

we approximate the free energy change (ΔG) with the internal energy change per intercalated lithium ion (ΔE), by taking the difference between the total energies of the reactants and the products:

$$\Delta G \approx \Delta E = (E_{\mathrm{PROD}} - E_{\mathrm{REACT}})/\text{no. of lithium atoms}$$

This approximation excludes effects of entropy and volume change. However, the contribution of the vibrational and configurational entropy terms to the cell voltage at room temperature is expected to be small (<0.1 V), and there is little change in volume during the intercalation. Even so, we appreciate that this is a significant approximation.

We estimate the change in internal energy by calculating the total energy, $E(x)$, of pure V_2O_5 and of three $\mathrm{Li}_x\mathrm{V}_2\mathrm{O}_5$ phases where $x = 0.5$, 1.0, and 2.0, and the total energy of pure lithium metal $E(\mathrm{Li})$. The change in the total energy of the system per intercalated lithium atom is given by

$$\Delta E(x') = \{E(x_2) - [E(x_1) + (x_2 - x_1)E(\mathrm{Li})]\}/(x_2 - x_1)$$

where $E(x)$ = total energy of $\mathrm{Li}_x\mathrm{V}_2\mathrm{O}_5$, $x_2 > x_1$, and $x' = (x_1 + x_2)/2$. Ideally, very small changes in composition could be used to calculate ΔE accurately, but this would require an unfeasibly large simulation cell.

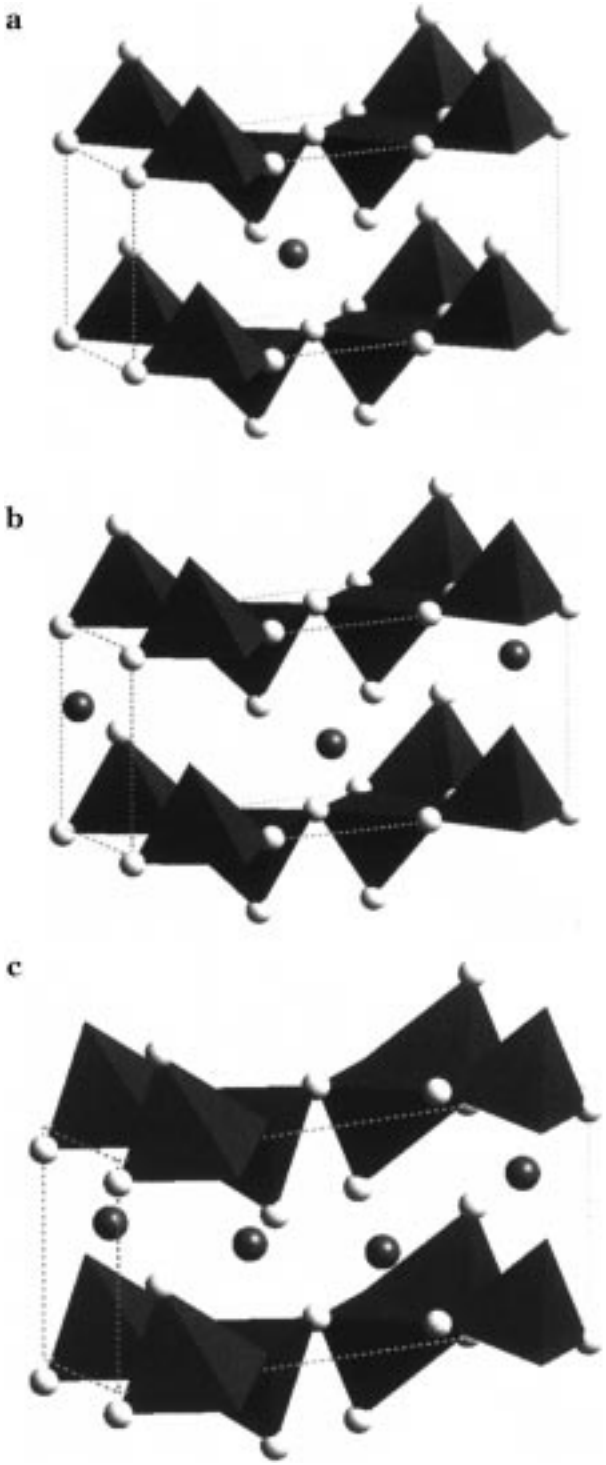

Figure 8. Optimized geometries of (a) $\mathrm{Li}_{0.5}\mathrm{V}_2\mathrm{O}_5$, (b) $\mathrm{LiV}_2\mathrm{O}_5$, and (c) $\mathrm{Li}_2\mathrm{V}_2\mathrm{O}_5$. Oxygen atoms are light gray while lithium atoms are darker. Vanadium coordination polyhedra are shown.

The resulting predicted average cell voltages are shown in Table 7.

The fine structure of the discharge curve, including the plateaux and steps seen in the experiment, cannot

(39) Deiss, E.; Wokaun, A.; Barras, J.-L.; Daul, C.; Dufek, P. *J. Electrochem. Soc.* **1997**, *144*, 3877−3881.

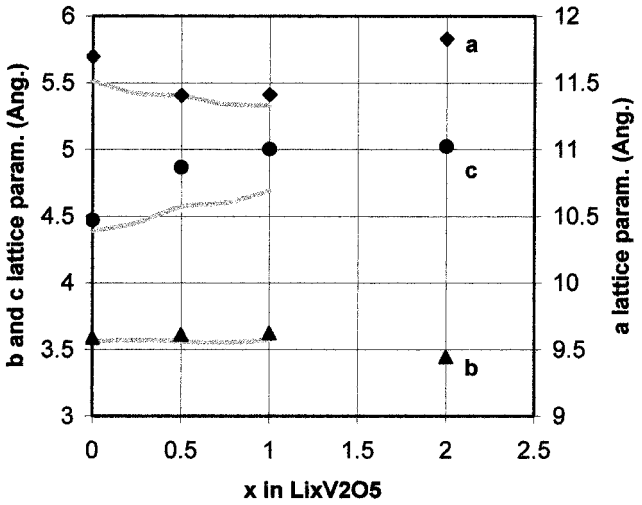

Figure 9. Experimental[20] and calculated unit cell dimension changes during lithium intercalation. Experimental data are shown in gray while calculated points are shown in black.

Figure 10. Key to vanadium atom numbering for charge distribution plots.

Table 6. Optimized Lithium Positions in $Li_xV_2O_5$ Phases

phase	lithium position
$Li_{0.5}V_2O_5$	0.5046, 0.1714, 0.3591
LiV_2O_5	0.4999, 0.1761, 0.3619

Table 7. Predicted Average Voltages and Experimental[3] Cell Voltages for the Li/V_2O_5 System

lithium concentration (x in $Li_xV_2O_5$)	cell potentials (V)	
	experimental	calculated average
0.25	3.4	3.0
0.75	3.2	1.8
1.50	2.2	1.5

be reproduced with the small number of $Li_xV_2O_5$ configurations that have been simulated so far. However, the predicted *average* cell voltages are in good general agreement with experimental values, although some consistent underestimation is observed. There is a larger discrepancy between the experimental and the calculated average value for $x = 1.5$ due to the steepness of the discharge curve around 1 V. This makes our predicted value, taken as the average between $Li_{1.0}V_2O_5$ and $Li_{2.0}V_2O_5$, less accurate. Consistent underestimation of cell discharge voltages by DFT methods is also noted by Aydinol et al.,[9] where it is proposed that the main error comes from the overestimation of the binding energy for lithium metal.

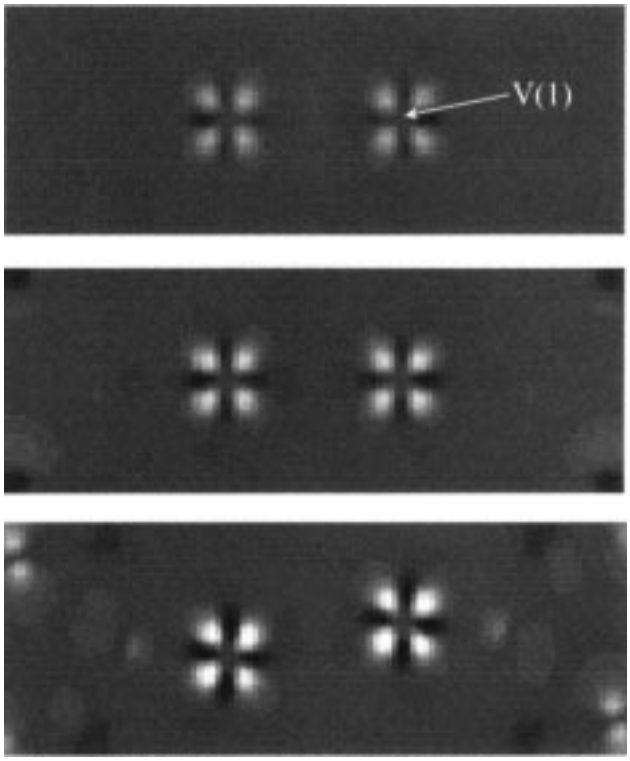

Figure 11. Charge density difference along the 001 direction, sliced through the two V(1) atoms: top, $Li_{0.5}V_2O_5$; middle, LiV_2O_5; bottom, $Li_2V_2O_5$.

4.4. Charge Distributions. As we have already noted, the intercalation of lithium must be accompanied by reduction of the host lattice, as the guest species is usually thought to be Li^+. We have investigated this problem by studying the calculated valence electron density distributions. By subtraction of the electron density distribution of the bulk oxide from the electron density distribution of the intercalated system, it is possible to calculate the distribution of the electrons due only to the intercalation reaction: the charge density difference distribution. This subtraction requires us to perform a simulation of the host V_2O_5 distribution for each $Li_xV_2O_5$ configuration using the same atomic positions and unit cell dimensions as the lithiated phases: this is done by removing the lithium ions from the optimized $Li_xV_2O_5$ systems and then carrying out a single point calculation on the distorted host lattice.

Before the results are presented, we should note that the intercalation of lithium produces the two inequivalent sets of vanadium atoms in the V_2O_5 unit cell that are shown in Figure 10, and which will be referred to in the following discussion.

The charge density difference distribution are given as gray scale plots in Figures 11−15, where white and light gray areas represent high and low levels of positive electron density respectively, zero density is shown in dark gray, and black areas represent negative electron density. The arbitrary scale runs from +90 (white) to −35 (black).

We find that the electrons that ionize from the lithium during the intercalation reaction are almost exclusively localized on the vanadium centers. In the $Li_{0.5}V_2O_5$ phase, the single electron that has been added per unit cell is more localized over the two V(1) centers, and not delocalized over all four metal atoms in the unit cell.

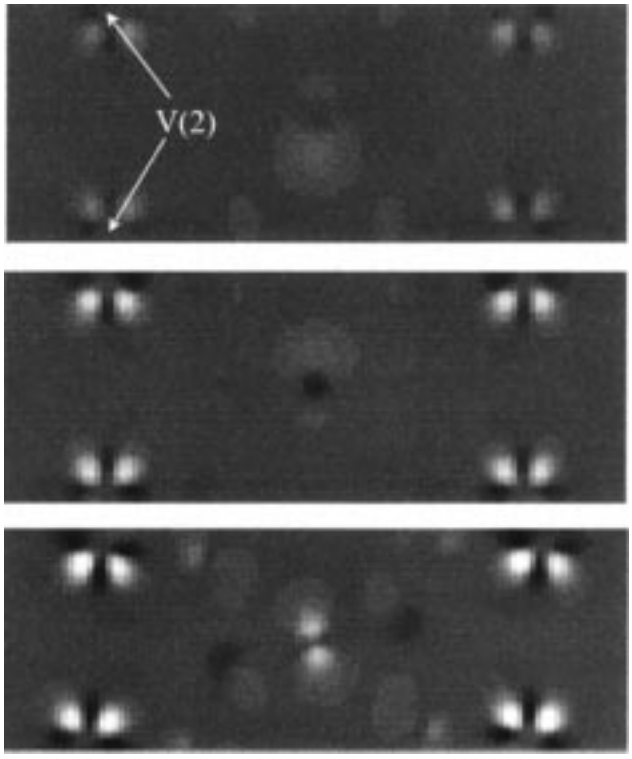

Figure 12. Charge density difference along the 001 direction, sliced through the two V(2) atoms(positioned at the edge of the slice): top, $Li_{0.5}V_2O_5$; middle, LiV_2O_5; bottom, $Li_2V_2O_5$.

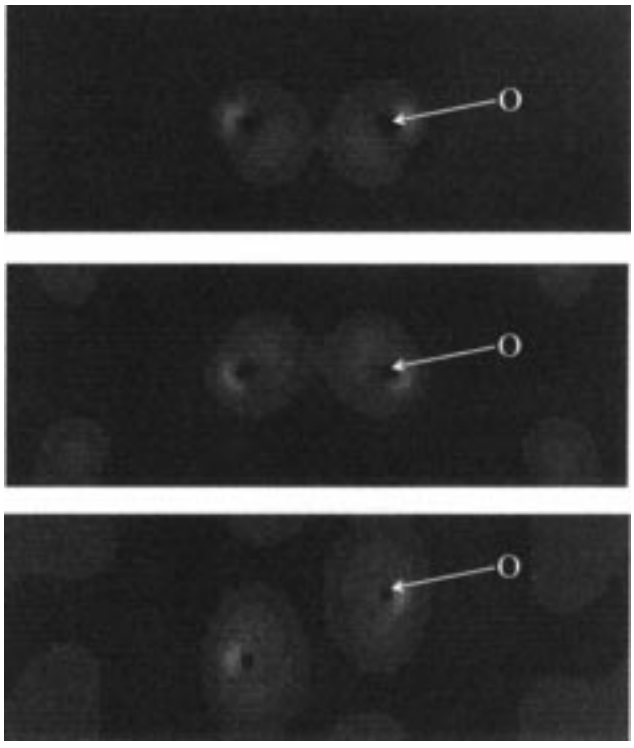

Figure 13. Charge density difference along the 001 direction, sliced through the two vanadyl O atoms: top, $Li_{0.5}V_2O_5$; middle, LiV_2O_5; bottom, $Li_2V_2O_5$.

The LiV_2O_5 and $Li_2V_2O_5$ phases, which contain two and four electrons per unit cell respectively, have an even distribution over all four vanadium centers, although we find that there is significantly more electron density around each V atom in $Li_2V_2O_5$. In every case, the electron density appears to populate a vanadium $\pi-$d orbital. We do see small amounts of positive electron density on the oxygen atoms, although this density is significantly less than that localized on the vanadium d orbitals.

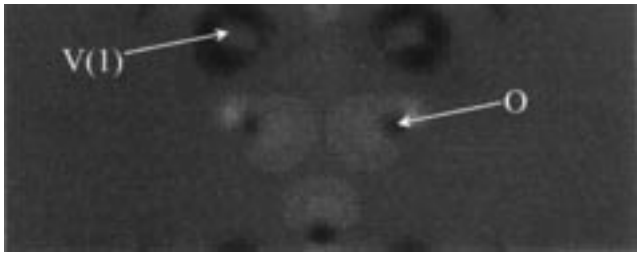

Figure 14. Charge density difference in LiV_2O_5 along the 010 direction, showing the loss of electron density along the vanadyl bonds.

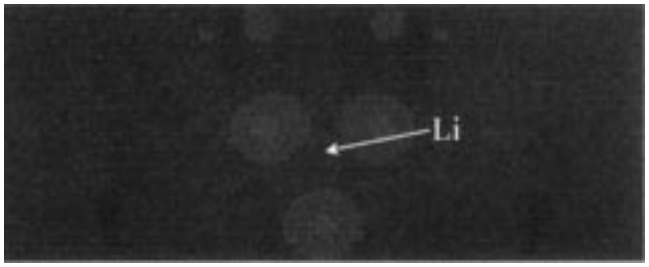

Figure 15. Charge density difference in LiV_2O_5 along the 010 direction, showing that the intercalated lithium is fully ionized.

Table 8. Optimized Vanadyl Bond Lengths in $Li_xV_2O_5$

phase	V═O (vanadyl) bond length (Å)
V_2O_5	1.607
$Li_{0.5}V_2O_5$, $V_{reduced}$═O	1.636
$Li_{0.5}V_2O_5$, $V_{unreduced}$═O	1.604
$Li_1V_2O_5$	1.641, 1.644
$Li_2V_2O_5$	1.717

The reduction of the vanadium centers is accompanied by a reduction in the electron density between the metal and the vanadyl oxygen, which is apparent as areas of negative density on the distribution maps when viewed along the *b* axis (Figure 14). The effect is to weaken and lengthen the vanadyl bond, which appears in the optimized geometries (see Table 8). Two vanadyl bond lengths are observed in $Li_{0.5}V_2O_5$, as some vanadium atoms are reduced, while others are not.

We find that the intercalated lithium is fully ionized in the host lattice. The Li centers are invisible on the electron density maps (Figure 15), showing that the valence electron due to lithium has been removed and that the guest species is Li^+.

4.5. Lithium Migration Processes. It has been noted in experimental studies that lithium migration takes place parallel to the *b* direction, along channels formed by the vanadyl bonds; this migration route has consequently been investigated using potential based static lattice simulation techniques.

To study the energetics of lithium mobility in V_2O_5, we have undertaken a series of bulk optimizations on intercalated V_2O_5, using interatomic potential based methods. By constraining the position of the lithium atom by keeping its position in the *b* direction constant throughout the optimization, it is possible to optimize the position of the ion in the $a-c$ plane. By carrying out a series of calculations, with the Li^+ ion at different positions along the *b* cell parameter, it is possible to

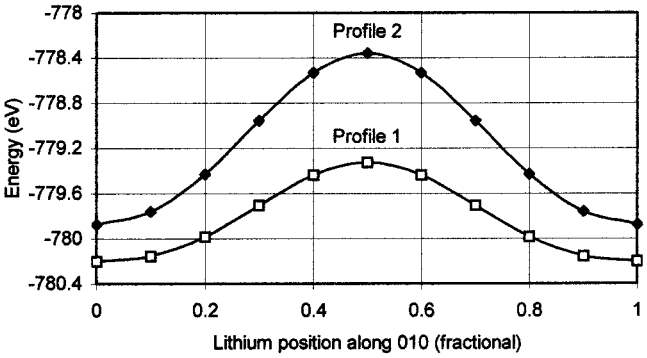

Figure 16. Energy profiles for lithium migration through V_2O_5: profile 1, reduced V(IV) species is V(1) at 0.351186, 0.500000, 0.891700; profile 2, reduced V(IV) species is V(2) at 0.148812, 0.000000, 0.108300

Figure 17. Lithium migration path through V_2O_5 for profile 1. Only the first half of the path is shown (from $b = 0.0$ to $b = 0.5$).

construct the potential energy path for the lithium ion as it moves along this axis.

One of the vanadium atoms in the bulk lattice must be reduced as the optimization requires that the total charge on the cell is zero. If one lithium ion is incorporated per unit cell, then there are two inequivalent V atoms in the crystal structure (V(1) and V(2) in Figure 11), so an energy profile has been calculated for both choices of reduced cation. For each optimization, which is carried out at constant volume, the initial position of the lithium in the *a* and *c* directions, before geometry optimization, is identical: expressed as fractional coordinates these are 0.500 along *a* and 0.350 along *c*. It is necessary to constrain some of the vanadium atom positions to stop the whole of the bulk lattice moving, relative to the lithium ion, along the *b* lattice parameter during the optimization. This has been done by holding the position of one V atom constant in all directions, which effectively anchors the system, while all other vanadiums are constrained only along the *b* direction. Although we appreciate that this does prevent a full optimization of the vanadium positions, we found it was the only way to stop the Li^+ ion from moving back to its most stable position during each optimization. The predicted energy profiles are shown in Figure 16 and the migration paths are given in Figure 17.

We find that the position of the reduced vanadium center has a significant effect on the energy profile of the lithium migration and the overall activation energy for the process. A lower activation energy, of 0.88 eV compared to 1.52 eV, is predicted when the V^{IV} species is, on average, closer to the lithium ion, which can also be rationalized in terms of the distance between the Li^+ and the reduced vanadium ions. The barrier in path 2 is reduced in path 1 because the lithium is closest to the V^{IV} center at this point in the migration pathway. The actual route taken by the Li^+ ion is similar in paths 1 and 2; the curve in both paths may, in part, be caused by the V^{IV} center being to one side, especially in the a direction.

The findings from the atomistic calculations that the activation energy of lithium migration through V_2O_5 is dependent on the position of the V(IV) center in the lattice is supported by the calculated DFT electronic distribution in $Li_{0.5}V_2O_5$. These electronic structure results indicate that the vanadium atoms closest to the lithium path are reduced in preference to those further away; the atomistic simulation predicts a lower activation energy if this is the case.

5. Conclusions

The first significant finding of this study is that atomistic defect calculations can be used to locate successfully stable, low-energy, sites for intercalated lithium in the V_2O_5 lattice. The resulting lithium coordinates may be used to give the initial geometries for the electronic structure studies; we find that they give a good estimate of the lithium position in the $Li_xV_2O_5$ phases ($x \leq 2$). Interatomic potential-based modeling has also been used to show that lithium is mobile along the channel in the *b* direction in V_2O_5, with a calculated activation energy of 0.88 eV.

Our electronic structure calculations of the $Li_xV_2O_5$ system, for $x = 0.5$, 1, and 2, have given structures which are in good agreement with experiment and total energies which can be used successfully to predict *average* cell voltages. Our calculated charge density maps show that the vanadium centers are reduced during the intercalation reaction, and that the additional electrons are not localized on a single metal atom but appear to enter a band due to the vanadium $\pi-$d orbitals. The calculated electron densities suggest that intercalated lithium is fully ionized and that reduction of the vanadium centers leads to a weakening of the vanadyl bond—an effect that is reproduced in the calculated vanadyl bond lengths.

Further work will concentrate on the predictions of variations in cell voltages for the Li/V_2O_5 system, a problem of major industrial importance. Indeed, the successful simulation of the chemical processes taking place at the cathode of all lithium batteries is of great importance in the search for new and improved electrode materials.

Acknowledgment. We wish to thank Georg Kresse at Technical University Vienna for kindly giving us permission to use the VASP code in this work. J.S.B. would like to thank Dr G. Morrison for his assistance with some of the electron density work and Prof. P. E. Ngoepe, of The Materials Modeling Centre, University of the North (UNIN), Pietersburg, South Africa, for his hospitality and help. We are grateful to the EPSRC for the funding of computational facilities at Royal Institution of Great Britain and a studentship for J.S.B. The Royal Society and FRD (South Africa) are thanked for funding the visit of J.S.B. to UNIN.

CM980735R